

## Photoinduced magnetic effects in amorphous spin glasses

M. Ayadi

*Faculté des Sciences de Tunis, 1060 Tunis, Tunisia*

*and Laboratoire de Physique des Solides, Bâtiment 510, Université Paris-sud, 91405 Orsay CEDEX, France*

J. Ferré\*

*Laboratoire de Physique des Solides, Bâtiment 510, Université Paris-sud, 91405 Orsay CEDEX, France*

(Received 15 March 1991)

We report on photoinduced magnetic phenomena in amorphous insulating spin glasses, the cobalt and manganese aluminosilicate glasses, below their freezing temperature. The homogeneity of the samples has been checked by electron microscopy. X-ray and optical-absorption measurements proved that manganese and cobalt ions are only in their divalent state. This photomagnetism cannot be interpreted by previously developed theories for other magnetic crystalline materials. A semiphenomenological theory, which assumes a pseudolocalized character of the photoinduced magnetic effects, is proposed to interpret the experimental data. All experimental results on the temperature, magnetic-field, and light-wavelength dependences of the effect strongly support the hypotheses put forward in our model. The proposed microscopic origin of the phenomenon deals with localization of nonthermalized phonons, created during the optical excitation of the  $3d$  metal ions in the investigated amorphous compounds. Magnetic frustration in these spin glasses also limits the extension of the magnetically perturbed region.

### I. INTRODUCTION

Magnetic garnets were the first compounds in which variations of magnetic properties under light illumination were observed.<sup>1</sup> This phenomenon, also referred to as photomagnetism or photoinduced magnetic effects,<sup>2</sup> has been found to occur in other classes of magnetic materials such as doped  $\text{CdCr}_2\text{Se}_4$ ,<sup>3</sup> ferrites,<sup>4</sup> and  $\text{FeBO}_3$ .<sup>5</sup> The interpretation of the photomagnetism in these compounds is related to the presence of magnetic ions with two valence states. Then, the absorption of photons may induce a charge transfer between magnetic ions in different valence states localized in neighboring sites; this drives variations of some magnetic properties of the sample. Other photoinduced effects can be evidenced on several optical properties such as the apparition of a linear dichroism<sup>6</sup> or the modification of the absorption coefficient under illumination<sup>7</sup> which are sensitive to the change of the local anisotropy induced by light.

As we shall see later, the photoinduced magnetic effect we discovered in the spin-glass state of cobalt and manganese aluminosilicate glasses<sup>8-10</sup> under weak light illumination cannot be interpreted within the above mechanism. We shall stress that this effect is closely related to the amorphous magnetic structure of these insulating spin glasses. Very recently photoinduced magnetic effects were also evidenced in the spin-glass state of amorphous metallic alloys<sup>11</sup> extending the generality of such an effect to all kinds of magnetic glasses. The aim of this paper is to study the influence of pertinent parameters (temperature, light intensity and wavelength, magnetic field, etc.) on the photomagnetism in these aluminosilicate glasses in order to state unambiguously the simple semiphenomenological theory we previously introduced<sup>8</sup>

and finally to propose a related microscopic mechanism. We wish to justify our model starting from chemical and structural analyses of these glasses, reported in Sec. II. In Sec. III we summarize their useful magnetic properties. The presentation of the main characteristic features of this photoinduced magnetic effect is given in Sec. IV. In order to justify the hypotheses used to develop our model in Sec. V, a general discussion is proposed in Sec. VI.

### II. STRUCTURAL ANALYSIS AND SAMPLE CHARACTERIZATION

#### A. Preparation and homogeneity

The studied cobalt and manganese aluminosilicate glasses were prepared by de Graaf and Wenger<sup>12</sup> (Wayne State University) and Knorr<sup>13</sup> (University of Tübingen), respectively. Thin platelets ( $e \sim 0.1$  mm) of cobalt aluminosilicate glasses have a blue color by light transmission which reveals the presence of Co(II) in a tetrahedral oxygen environment. On another hand, the manganese aluminosilicate glasses are highly transparent even under thicknesses of more than 1 cm and show a brown-pink color. As we shall see later, this proves that the Mn(II) sees an octahedral oxygen environment. The nominal compositions of the samples studied in this work are reported in Table I. In the following we shall use the shortened notations mentioned in this table to refer to the different samples.

The preparation of these compounds exhibits some difficulties, especially for cobalt glasses. Verhelst *et al.*<sup>12</sup> invoked large chemical fluctuations and even discussed about phase separation in highly concentrated cobalt

TABLE I. Compositions of samples and studies undertaken in this work. The asterisk denotes studies done on any sample.

Compounds	Composition	Concentration of magnetic ions		Physical measurements				$T_{f_0}$ (K)
		(at. %)	Shortened notation	Magnetic	Optical absorption	x-ray absorption	Fluorescence	
Cobalt glasses	$(\text{CoO})_{0.4}(\text{Al}_2\text{O}_3)_{0.2}(\text{SiO}_2)_{0.4}$	13	CoAS 13	*	*	*		5
	$(\text{CoO})_{0.6}(\text{Al}_2\text{O}_3)_{0.1}(\text{SiO}_2)_{0.3}$	23	CoAS 23	*	*			
Manganese glasses	$(\text{MnO})_{0.35}(\text{Al}_2\text{O}_3)_{0.1}(\text{SiO}_2)_{0.55}$	12	MnAS 12	*	*	*	*	2.1
	$(\text{MnO})_{0.428}(\text{Al}_2\text{O}_3)_{0.144}(\text{SiO}_2)_{0.428}$	15	MnAS 15	Magneto-optic *	*	*	*	2.85
	$(\text{MnO})_{0.5}(\text{Al}_2\text{O}_3)_{0.1}(\text{SiO}_2)_{0.4}$	18.5	MnAS 18	Magneto-optic *	*	*	*	~4

glasses ( $c > 33$  at. % Co), which are not investigated in the present work. To elucidate this point, we checked qualitatively and quantitatively the homogeneity of the CoAs 13 sample, taken as an example, at several length scales.

The high degree of amorphism of cobalt and manganese aluminosilicate glasses prevents upon the presence of microcrystallites, as often evidenced in iron aluminosilicates. Our cobalt sample, cut and optically polished as a thin plate ( $e \sim 0.1$  mm), was selected after examination with an optical microscope in order to ascertain its macroscopic homogeneity. The quantitative composition analysis of some parts of the sample has been done afterwards by using scanning electron microscopy by reflexion. We checked the good homogeneity of our sample at the micron scale, the deviations in composition being estimated to less than 1%. Another observation on a 0.1- $\mu\text{m}$ -thick specimen by transmission electron microscopy (Phillips 100 keV microscope EM 300) allowed us to eliminate the hypothesis of a phase separation at a 0.1  $\mu\text{m}$  scale.

In a last stage, we checked its homogeneity at a higher resolution by using a scanning transmission electron microscope (STEM). An analysis of the x-ray backscattering has permitted us to determine the nominal concentration of most of the elements entering the glass over a scale of  $10^{-2}$   $\mu\text{m}$ . Finally, by means of the loss energy spectrum, we established the mapping of the cobalt and oxygen ions over an area of about  $1000 \times 1000 \text{ \AA}^2$  with a spatial resolution of 10  $\text{\AA}$ . The obtained picture (Fig. 1) shows a rather uniform intensity of the two elements over the whole sample area which rules out the presence of large fluctuations in composition down to typical sizes of 100  $\text{\AA}$ .

Summarizing these studies, we prove that our selected CoAS 13 samples are highly homogeneous over an extended spatial scale, down to 100  $\text{\AA}$ .

#### B. Local structure and valence state of manganese and cobalt

Only few studies<sup>14-17</sup> were reported on the structure and on the valence state of the metallic ion in such highly concentrated aluminosilicate glasses. Their magnetism and photomagnetism have to be understood considering

their chemical and structural properties. The local structure in these glasses cannot be determined by electron paramagnetic resonance (EPR)<sup>18</sup> because of the excessively large magnetic exchange interaction. The degree of oxidation and the coordinance of cobalt and manganese ions were deduced from absorption spectra in the visible or x-ray ranges. Nevertheless, these methods give information only on the very short-range order because of the excessively large topological disorder existing in these concentrated glasses.

#### 1. Analysis of the optical spectra

The room-temperature absorption spectra of the two studied cobalt aluminosilicate glasses CoAs 13 and 23, shown in Fig. 2, are typical of the cobalt in its divalent state. Cobalt glasses melted under nonoxidizing conditions are well known to contain only Co(II) and from the energy of bands of the absorption spectra, we can confirm this valence state and exclude the presence of Co(III).

The Co(II) ions generally occupy either octahedral or tetrahedral sites. For the two types of sites, the absorption bands are expected to appear in the same spectral range. However, the rather large oscillator strength of the absorption bands located in the visible and near infrared, as for  $\text{Co}^{2+}$ -doped ZnO or ZnS crystals,<sup>19</sup> points out that Co(II) occupies mainly tetrahedral sites, without

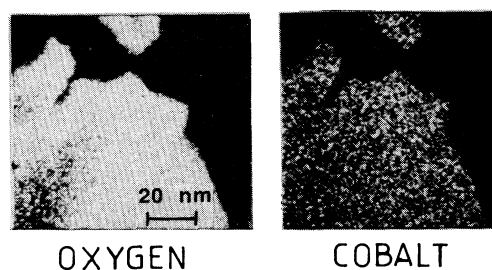


FIG. 1. Distribution of oxygen and cobalt (13 at. %) atoms in CoAS 13 (STEM measurements). The short-range contrast is mainly due to the noise.

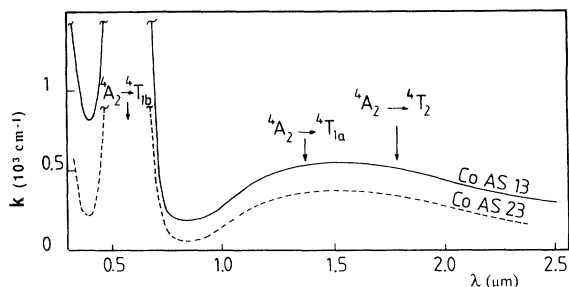


FIG. 2. Room-temperature optical-absorption spectra of the cobalt aluminosilicate glasses. The assignment of the absorption bands of Co(II) in a tetrahedral site symmetry is indicated.

excluding a possible mixing with octahedral coordination. This conclusion well agrees with the results of previous measurements of the cobalt magnetic moment for concentrations smaller than 20 at. %.<sup>12</sup>

As already discussed,<sup>15</sup> the absorption spectra of our manganese aluminosilicate glasses MnAs 15 and 18, shown in Fig. 3, reveal only the presence of Mn(II), opposite to other glasses obtained in more oxidizing conditions.<sup>14</sup> The weakness of the absorption intensity in the spectral range 0.45–0.60  $\mu\text{m}$  is only consistent with a centrosymmetric environment of the manganese (assumed octahedral). The high intensity of the absorption bands located around 0.42  $\mu\text{m}$  ( ${}^6A_{1g} \rightarrow {}^4A_{1g}, {}^4E_g$ ) and 0.35  $\mu\text{m}$  ( ${}^6A_{1g} \rightarrow {}^4E_g, {}^4T_{2g}$ ) is well understood considering an electric dipole exchange mechanism.<sup>15</sup>

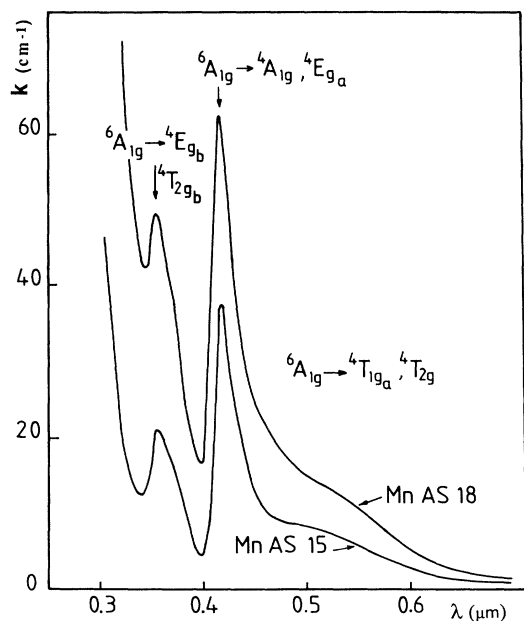


FIG. 3. Room-temperature optical-absorption spectra of two manganese aluminosilicate glasses. The assignment of the absorption bands of Mn(II) in an octahedral site symmetry is indicated.

In the studied aluminosilicate glasses, from the light absorption measurements, we show that manganese and cobalt are in their divalent state. The manganese ions are only located in centrosymmetrical sites (assumed octahedral) while at least a large amount of cobalt ions occupies tetrahedral sites.

## 2. Analysis of the x-ray absorption spectra

X-ray absorption in manganese and cobalt aluminosilicate glasses was performed with synchrotron electromagnetic radiation, delivered by the DCI storage ring at Orsay (LURE). Absorption spectra were obtained in a thin, polished platelet ( $e = 70 \mu\text{m}$ ) of CoAS 13. Considering the higher intrinsic absorption of the manganese we used a sample composed of a few stacked homogeneous layers of MnAs powder.

Experiments were performed in the vicinity of the  $K$  absorption edge of the cobalt or manganese elements. The shape and position of the absorption edge are related to the oxidation state of the studied element, the metal-oxygen covalency, and the local symmetry. For CoAs 13, the prepeak localized at about 10 eV below the Co  $K$  edge (Fig. 4) may be assigned to a forbidden  $1s \rightarrow 3d$  transition which is clearly enhanced by the hybridization of  $3d$  Co with  $2p$  O orbitals due to the noncentrosymmetric environment of the metal ion. The prepeak positions and the  $K$ -edge energies are identical for our cobalt glass and for the investigated cobalt chromite crystals (Fig. 4 inset). This demonstrates again that the local site symmetry for cobalt in the glass is mainly tetrahedral as for the chromite.

Above the  $K$  absorption edge, the analysis of the extended x-ray absorption fine structure (EXAFS) allowed us to determine the mean distances between a cobalt and other neighboring atoms. However, EXAFS gives preferential information on shorter distances. The EXAFS spectrum of CoAS 13 (Fig. 4) shows a damped sinusoidal

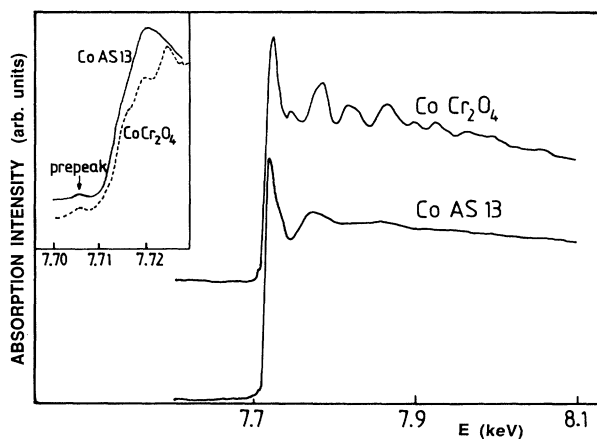


FIG. 4. Room-temperature x-ray absorption spectra on the  $K$  edge of cobalt for the aluminosilicate glasses CoAS 13 and the cobalt chromite. EXAFS are oscillations in the 7.72–8.10 keV range. Inset: details at the edge with a resolution of 1.5 eV. We clearly distinguish the prepeaks around 7.705 keV.

shape, which is less structured than that of the cobalt chromite crystal. This damping comes from the dispersion of the atomic distances associated with the topological disorder. From the Fourier transform of EXAFS oscillations we deduced the radial distribution function of pairs of atoms having a cobalt ion as the origin (Fig. 5). In the analysis procedure, the value of the absorption edge was taken as an adjusting parameter. The higher peak is assigned to the first layer of oxygen atoms surrounding a cobalt. The mean distance Co-O is found to be 1.98 Å as for the cobalt chromite crystal, confirming unambiguously the fourfold coordination of cobalt in CoAs 13. The identification of other shoulders and peaks in the radial distribution is more ambiguous.

Consistent with our previous conclusion that manganese lies at centrosymmetric sites, no prepeak can be detected on x-ray spectra near below the *L*-absorption edge for MnAs 12, 15, and 18 samples (Fig. 6). From their EXAFS spectra, which are rather similar, we deduce the radial distribution around one manganese and determine the same Mn-O first-neighbor distance of 2.04 Å for all the three samples. This distance is far shorter than that of 2.14 Å determined for octahedral distorted sites in  $\text{MnCO}_3$  and disagrees with Mn-O separations determined for pure octahedrally coordinated crystals like MnO (2.22 Å) and  $\alpha\text{-Mn}_2\text{SiO}_4$  (2.21 Å). Such shortening of the metal-oxygen distance has already been reported in several glasses<sup>16</sup> since EXAFS could give the shorter limit of its asymmetric distribution.

The MnAS 15 glass has the same nominal composition as the spessartite crystal. However, in the garnet structure of spessartite, divalent manganese occupies eightfold-symmetry sites. As mentioned previously,<sup>16</sup> the change of coordination between the glass and the crystalline compound is related to important structural

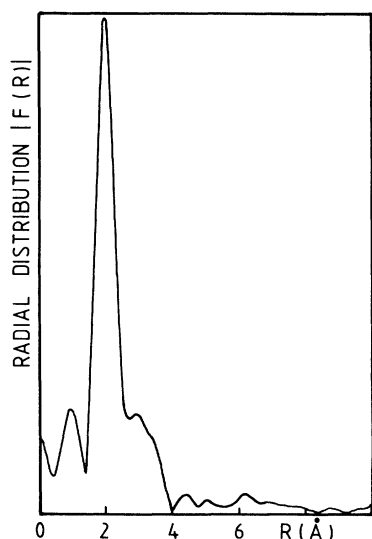


FIG. 5. Radial distribution of atoms around one cobalt in CoAS 13 deduced by Fourier transform of the EXAFS spectrum.

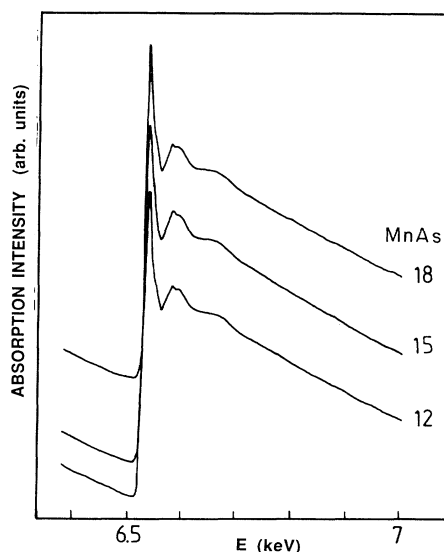


FIG. 6. Room-temperature x-ray absorption spectra on the *K* edge of manganese (12,15,18 at.%) for the aluminosilicate glasses MnAS 12, 15, and 18.

differences: polymerization of  $\text{SiO}_4$  tetrahedra and coordination change of Al atoms in the glass. Consequently, it is impossible to have a close comparison between their EXAFS spectra.

Unfortunately, the highly important atomic disorder prevents us to estimate independently the number of ions on each layer and to find other atomic separations from EXAFS spectra. X-ray absorption measurements confirm the tetrahedral oxygen environment in CoAS 13 and a centrosymmetric situation in manganese aluminosilicate glasses. Consequently, the ground states of the metal ions are orbitally quenched, leading to a small magnetic anisotropy in these glasses.

The cobalt and manganese oxides may be considered as the former in the glass network. The polymerization of CoO tetrahedra or MnO octahedra in open and closed chains in the glass can lead to a ramified character of the magnetic lattice. This generates the localization of frustrated magnetic bounds and can create unfrustrated clusters.

### 3. Fluorescence studies

The understanding of the microscopic origin of photoinduced magnetic effects in aluminosilicate glasses needs a deep knowledge of the dynamics in the optically excited states of the magnetic ions. In this paper, we shall summarize some conclusions of our studies in the manganese glasses. Fluorescence appears in the near infrared when the samples are excited by light in the absorption bands lying in the visible range (Fig. 3); more details on the light emission properties will be published elsewhere.<sup>20</sup> Since the cobalt glasses absorb up to  $\lambda=3 \mu\text{m}$  (Fig. 2), we were unfortunately not able, with our equipment, to perform similar fluorescence experiments

on CoAS samples.

The fluorescence of MnAS 15 and 18, undetectable at room temperature, increases strongly by lowering the temperature down to 4.2 K. This fact, associated with a quenching of the emission by increasing manganese doping, is consistent with an exchange assisted transfer of energy in the excited states. Consequently, at low temperature, the excitation remains localized around each excited magnetic ion. The nonexponential time decay of the fluorescence intensity well reveals the randomness in the local distribution of manganese sites, already found by EXAFS. At low temperature, the electron remains a long time in the excited states as revealed by the long fluorescence lifetime of few milliseconds. Then, light is able to induce strong changes of the local temperature and magnetic order in the excited states.

### III. SUMMARY OF MAGNETIC PROPERTIES

The aim of the first magnetic studies of these glasses was to investigate magnetism in amorphous antiferromagnets.<sup>12</sup> Later, more precise magnetic measurements<sup>21-23</sup> demonstrate that they may be considered as insulating spin glasses. The spin glass behavior manifests itself at low temperature in these glasses; it is due to the topological disorder which induces magnetic frustration.

Above 50 K, their ac magnetic susceptibility follows a Curie-Weiss law with high negative values of the paramagnetic Curie temperature  $\Theta_p \sim -100$  K,<sup>12,21</sup> consistent with large values of the antiferromagnetic exchange interaction. In the temperature range 50–10 K a new regime has been attributed to a superparamagnetic behavior,<sup>12,15</sup> related to the strengthening of short-range magnetic correlations between manganese or cobalt ions. Beauvillain *et al.*<sup>22</sup> have evidenced a critical divergence of the nonlinear susceptibility of MnAS 15 at the freezing temperature  $T_{f_0} = 2.95$  K, supporting the occurrence of a paramagnetic–spin glass transition for high concentrated manganese aluminosilicate glasses.

The situation is less obvious for CoAS glasses, for which the analysis of their dynamic magnetic properties<sup>23,24</sup> can be consistent with a progressive dynamic freezing of superparamagnetic clusters. However, recent measurements<sup>25</sup> on the magnetic relaxation related to temperature steps have revealed a great change of the dynamic properties at a well-defined temperature taken as  $T_{f_0}$ . The static freezing temperatures of the studied glasses are noted in Table I.

In spite of comparable values of the antiferromagnetic exchange interactions in manganese or cobalt glasses, the difference of the time scale involved in their dynamic properties can be understood by considering topological aspects. The octahedral coordinance of manganese in glasses favors a coupling between more magnetic ions, and consequently increases the density of frustration with respect to tetrahedrally coordinated cobalt glasses.

Refractive index measurements in MnAS glasses<sup>26</sup> ought to deduce the temperature dependence of their magnetic energy. This variation is rather smooth and can be fitted quite well within a one-dimensional Heisenberg model. This result is consistent with a polymeric

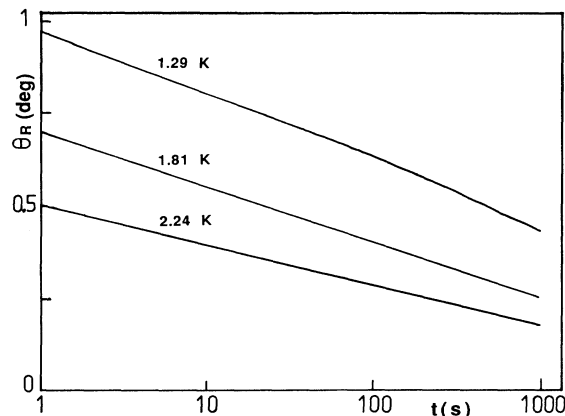


FIG. 7. Time dependence of the Faraday rotation ( $I_0 < 1 \mu\text{W}/\text{mm}^2$ ) assumed to be associated to the thermoremanent magnetization of CoAS 13 for several temperatures above the static freezing temperature  $T_{f_0} \sim 4$  K (error bars on the signal:  $\Delta\theta_R = 2 \times 10^{-3}$  deg). The value of the initially applied magnetic field was 7.5 kOe.

chain structure of manganese octahedra and is incompatible with crystallographic structure derived from garnets.

The variation of the relaxation of the thermoremanent magnetization (TRM), measured by Faraday rotation in CoAS 13 for several values of the temperature (Fig. 7), will serve in the discussion on the origin of the photoinduced magnetic effects. The magnetic-field dependence of the TRM, measured at a fixed time following the switching off of the field, exhibits a marked maximum (Fig. 8), as for well-known spin glasses.<sup>27</sup> This points out the collective behavior of the magnetization in the cobalt aluminosilicate glass below  $T_{f_0}$ .

### IV. THE PHOTOINDUCED MAGNETIC EFFECT

The relaxation of thermoremanent magnetization (TRM) induced after switching off the applied magnetic field, or of the aftereffect following the application of the

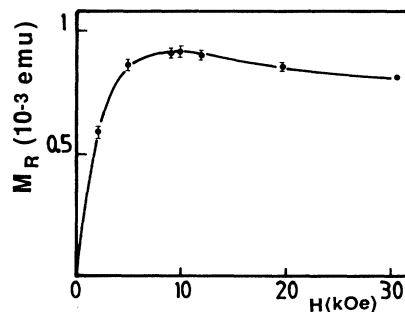


FIG. 8. Variation of the TRM in CoAS 13 with the value of the initially applied field, for  $t = 300$  s and  $T = 1.65$  K, deduced from extraction magnetic measurements.

field, were performed by Faraday rotation (FR).<sup>27</sup> The light beam propagated along the magnetic field direction. For the cobalt aluminosilicate glass CoAS 13, the specific FR ( $\theta/e$ ), measured with a laser diode ( $\lambda \approx 8400 \text{ \AA}$ ), was rather large and found to be proportional to the magnetization. On another hand, the specific FR, measured with a He-Ne laser in the manganese aluminosilicate glasses, was 3 orders of magnitude weaker than in the cobalt glasses, and found proportional to a linear combination of the magnetization and of the applied field, since the spin-orbit coupling is vanishingly small in the  $\text{Mn}^{2+}$  ground and excited states.<sup>28</sup>

By using two types of experimental setup we proved that, under light illumination, the change in FR was only due to that of the magnetization. In the first configuration I (Fig. 9), a method based on the modulation of the state of polarization (at 100 kHz) of the light allows an accurate measurement of the FR.<sup>27</sup> In this case, the light beam monitored in intensity by neutral density filters serves also to generate the photoinduced magnetic effect.

In the second configuration II (Fig. 9), we used two independent light beams, which are superimposed inside the sample, in order to separate the measurement of the FR from the light irradiation process. The intensity of the former FR light beam was kept as low as possible, typically  $1 \mu\text{W}/\text{mm}^2$ . The sample illumination may be monitored independently in intensity, polarization, and wavelength by a second beam emitted by another light source: a laser diode or an XBO xenon lamp coupled to a continuously variable spectral filter. A monochromatic filter was placed in front of the photomultiplier to eliminate only the remaining light flux coming from the second source.

The most spectacular demonstration of the photoinduced magnetic effect appears on the TRM relaxation,  $M_R(t)$ , of the studied glasses in their spin glass phase.<sup>8</sup> We recall that the TRM is obtained after first cooling the sample in a magnetic field through the freezing temperature  $T_{f_0}$  and then switching off the field at a temperature

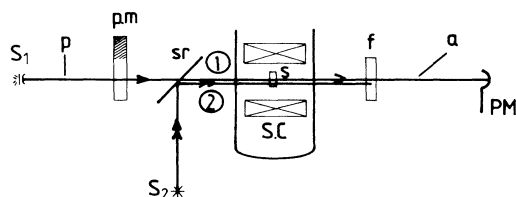


FIG. 9. Experimental arrangements used to study the photoinduced magnetic effects.  $S_1$ : laser diode source,  $p$ : polarizer,  $p.m$ : photoelastic modulator,  $s.r$ : semireflecting mirror,  $s$ : sample,  $SC$ : superconducting coil,  $f$ : narrow-band pass filter centered at the  $S_1$  wavelength,  $a$ : analyzer,  $PM$ : photomultiplier,  $S_2$ : second light source. In the configuration I, the FR light beam (1) could be monitored in intensity in the range  $1 < I_0 < 55 \mu\text{W}/\text{mm}^2$ . In configuration II, the FR light beam intensity (1) was  $1.5 \mu\text{W}/\text{mm}^2$  while the excitation intensity (2) could be adjusted in the range  $0 < I_0 < 200 \mu\text{W}/\text{mm}^2$ .

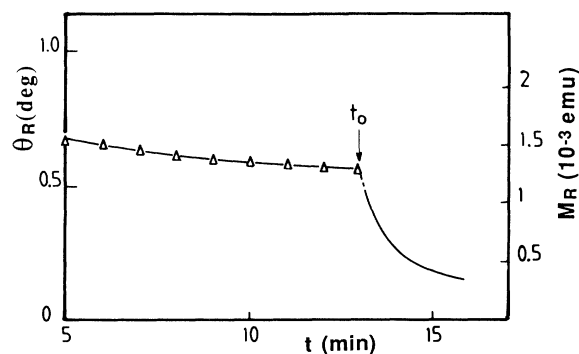


FIG. 10. For  $t < t_0$ : time dependence of the thermoremanent Faraday rotation (left ordinate) of CoAS 13 ( $e = 160 \mu\text{m}$ ) at 1.29 K ( $T/T_{f_0} \sim 0.26$ ) and of the corresponding calculated TRM (right), after magnetization under 4 kOe. In order to draw out only the thermal relaxation, we have rapidly measured the FR for discrete values of the time ( $\Delta$ ) under a weak light intensity of  $1.5 \mu\text{W}/\text{mm}^2$ . A drastic change in the relaxation appears after lighting the sample ( $\lambda = 8330 \text{ \AA}$ ) at  $t = t_0$ , following the switching of the field at  $t = 0$ , with an intensity of  $100 \mu\text{W}/\text{mm}^2$ .

$T < T_{f_0}$ . Afterwards, the TRM relaxes back very slowly to zero. As shown in Fig. 10, a sudden variation of the light intensity in configuration I turns out an instantaneous acceleration of relaxation of the thermoremanent FR of the CoAS 13 sample. This effect is irreversible since the reduction of the FR after illumination cannot be raised again by switching off the light or after decreasing the temperature.

We evidenced a similar photomagnetic effect in the manganese aluminosilicate glass MnAS 18<sup>10</sup> using the second arrangement II (Fig. 11) to get an efficient light irradiation from the second source ( $\lambda = 4780 \text{ \AA}$ ), i.e., in a region of high absorption of the sample (Fig. 3). The photoinduced magnetic effect has been evidenced in all samples reported in Table I but, in the following, we shall

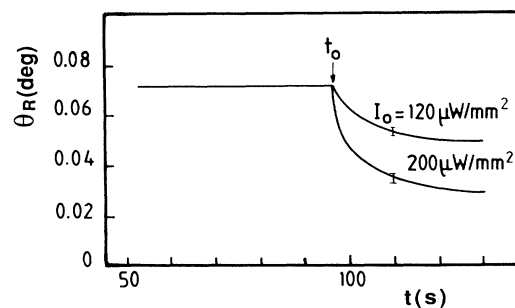


FIG. 11. Thermoremanent ( $t < t_0$ ) and photoinduced thermoremanent Faraday rotation ( $t > t_0$ ) of MnAS 18 ( $e = 6 \text{ mm}$ ) at 1.29 K, measured with an attenuated He-Ne laser beam ( $\lambda = 6328 \text{ \AA}$ ), after cooling the sample in  $H = 7.65 \text{ kOe}$ . At time  $t_0$ , the sample is irradiated by a second overlapping argon laser light beam ( $\lambda = 4780 \text{ \AA}$ ) with intensity  $I_0$ .

restrict the analysis to CoAS 13.

In fact, the photoinduced magnetic effect manifests itself not only on the relaxation of the TRM but also on all dynamic magnetic properties of these compounds. For example, light irradiation of magnetized samples fastens drastically the magnetic aftereffect process. This is illustrated in Fig. 12 for CoAS 13; the FR associated to in-field magnetization after zero-field cooling reaches more rapidly its equilibrium value under sample illumination, in a similar manner as the modification of the FR related to the TRM. The change of the dynamic behavior is also revealed on ac susceptibility,<sup>9</sup> measured by a derived magneto-optical method. The susceptibility, measured at 1 kHz, is significantly enhanced under illumination, a fact consistent with the increase of the relaxation rate.

Finally, it is interesting to note that the difference between the acquisition processes (field cooled or zero field cooled) for the remanent magnetization (either TRM or IRM)<sup>29</sup> becomes purely formal under light irradiation since the system reaches rapidly the equilibrium magnetization state; this simplifies considerably the experimental procedure to initialize again the magnetization. Typically, starting from a zero-field-cooled state, and after applying the magnetic field during some minutes to an illuminated sample with a light beam intensity of about 0.1 mW/mm<sup>2</sup>, we get the same magnetization as that generated by a field-cooled process.

We excluded sample heating as the origin of such drastic magnetic changes. The assessment of the increase of lattice temperature at equilibrium under a light intensity of 0.1 mW/mm<sup>2</sup> and for a 0.16-mm-thick sample of CoAS 13 is indeed smaller than 10<sup>-2</sup> K, as calculated from the known values of the thermal conductivity and absorption coefficient of the glass. As shown in Fig. 7, the corresponding relative decrease in thermoremanent FR,  $\Delta\theta_R/\theta_R$ , could not exceed 10<sup>-2</sup> for the most intense irradiation, i.e., a small variation compared with the

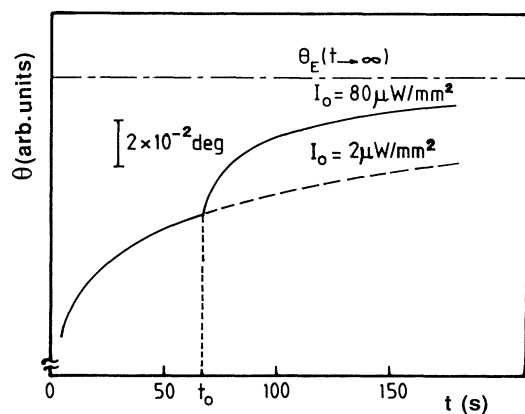


FIG. 12. Variation of the Faraday rotation ( $\lambda = 8100 \text{ \AA}$ ) corresponding to the TRM ( $t < t_0$ ) and to the photoinduced magnetic aftereffect ( $t > t_0$ ) in CoAS 13 ( $e = 70 \text{ \mu m}$ ), at 1.4 K, after a zero-field-cooled process and under  $H = 3.85 \text{ kOe}$ .  $\theta_E(t \rightarrow \infty)$  corresponds to the field-cooled magnetization value.

jump in magnetization reported in Fig. 10. A direct proof of the weakness of the temperature enhancement of the sample under irradiation is pointed out from the similar value of the freezing temperatures, corresponding to the maximum in susceptibility, under different light beam intensities.<sup>9</sup>

Let us point out that the photomagnetic effect in these glasses is never accompanied by other induced effects, as reported in better known cases.<sup>6</sup> For example, we checked that the optical absorption coefficient, measured at the excitation wavelength, is not affected within our accuracy ( $\Delta k/k < 10^{-3}$ ) by a significant modification of the intensity ( $I_0 < 0.2 \text{ mW/mm}^2$ ). The photoinduced magnetic effect also does not depend on the state of polarization of the irradiation beam. An unpolarized or a linearly polarized irradiation gives rise to a similar effect and a usual optical pumping is excluded since circularly right- or left-hand polarized light wave has the same photoinduced efficiency in spite of axial symmetry of the magnetized system.

An important property that will be useful later to state a theoretical model is the pseudolocalized character of this photoinduced magnetic effect. A crude experiment consists in following the change of the TRM relaxation on a small area of the sample induced by light illumination on a nonoverlapping region. The experimental arrangement is that described in configuration II, the second beam being focused on the sample; a double diaphragm with two pinholes of 0.5 mm diameter separated by 0.25 mm is positioned in front of the sample to guarantee the whole separation between the two light beams. We do not observe any modification of the relaxation rate of the TRM even for large irradiation intensities up to 0.2 mW/mm<sup>2</sup>. This experiment demonstrates the localized character of the photoinduced effect, at least at this scale.

A microscopic theoretical treatment of this phenomenon would require a better knowledge of the spin freezing in spin glasses, particularly in our amorphous compounds. For this purpose, the magnetic and crystallographic structures ought to be better identified, which is far to be realized. So in the following, by considering some characteristics of this effect and from a rough structural knowledge of these compounds, we have developed a semiphenomenological theory of this phenomenon. We shall discuss later, in Sec. VI, on its plausible microscopic origins.

## V. SEMIPHENOMENOLOGICAL TREATMENT OF THE PHOTOINDUCED MAGNETIC EFFECTS

The model we developed here is based on the pseudolocalized response of the magnetic system to the optical excitation, as already experimentally demonstrated above at a millimeter scale. This hypothesis is justified at a shorter scale since only amorphous spin glasses exhibit photomagnetic effects. Additional proofs of this localization will be given in the following. As we shall see later, the photomagnetic effects are not related to a specific absorption band but depend only on the absorption coefficient which is then taken as a pertinent parameter in the theory.

The optical excitation induces a weak magnetic perturbation which remains localized in regions with typical sizes related to that of the intrinsic magnetic inhomogeneities associated with topological disorder of the magnetic lattice, as mentioned in Sec. II A. The description of the dynamic properties of real glasses and spin glasses at low temperature usually involves a local behavior. Many authors consider an assembly of two-level systems to describe the glass properties.<sup>30</sup> An essential point in this approach is to specify the physical nature of these two-level systems without prejudicing upon the cooperative spin behavior, necessarily involved to explain the spin glass freezing process.<sup>29,30</sup> The photomagnetism in amorphous spin glasses is then described introducing a finite "magnetic dynamic correlation length" which characterizes the mean distance from the excited metal ion over which spins are affected during the photoinduced relaxation process.<sup>8</sup> We distinguish this "dynamic correlation length" from static correlations since the propagation of the short-lived perturbation is limited by the complexity of the magnetic lattice.

The theoretical model can be developed formally considering that the system is formed by a partition of real or virtual independent "magnetic clusters." A real one has physical boundaries, as for clusters of chemical origin. A virtual cluster may be defined by the finite spatial extension of the optically induced perturbation related to intrinsic defects in the amorphous lattice. Such notion will be justified later from the magnetic-field dependence of the effect. We have generalized our previous treatment<sup>8</sup> on the time dependence of the TRM to the case where the sample is illuminated at a time  $t_0$  which differs from the time  $t$  elapsed after switching off the magnetic field. If  $M_R(t)$  represents the relaxation of the TRM in darkness, for  $t > t_0$ , we can write

$$M(t-t_0) = \frac{M_R(t)}{\alpha d} \int_{\tau_{\min}}^{\tau_{\max}} \exp\left(\frac{t-t_0}{\tau}\right) \frac{d\tau}{\tau} \quad (1)$$

if  $\alpha$  is the absorption coefficient of the sample of thickness  $d$  and with

$$\tau_{\min} = \frac{1}{NwI_0}, \quad \tau_{\max} = \frac{\exp(\alpha d)}{NwI_0}, \quad (2)$$

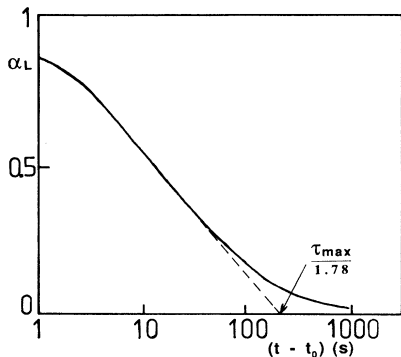


FIG. 13. Time dependence of  $\alpha_L$  calculated from expression (1) with particular values of  $\alpha d = 5.6$ ,  $\tau_{\min} = 1$  s,  $\tau_{\max} = 400$  s.

$N$  representing the mean number of magnetic ions in a "magnetic cluster,"  $w$  stands for the atomic cross section, and  $I_0$  is the value of the incident light intensity.

A similar treatment can be developed to explain the photoinduced changes of the in-field magnetic after-effect.  $M_R(t)$  in expression (1) has to be replaced by  $[M(H, t \rightarrow \infty) - M(H, t)]$ ,  $M(H, t)$  being the magnetization at a time  $t$  after switching on the field.

For the TRM the photoinduced relaxation coefficient can be defined by

$$\alpha_L(t-t_0) = \frac{M(t-t_0)}{M_R(t)}. \quad (3)$$

It reduces to the following asymptotic expressions:

$$\begin{aligned} \alpha_L((t-t_0) \ll \tau_{\min}) &= 1 - \frac{NwI_0}{\alpha d} [1 - \exp(-\alpha d)](t-t_0), \\ \alpha_L(\tau_{\min} \ll (t-t_0) \ll \tau_{\max}) &= 1 - (1/\alpha d)[0.577 + \ln NwI_0 - \ln(t-t_0)], \\ \alpha_L((t-t_0) \gg \tau_{\max}) &= \frac{1}{\alpha d} \frac{\exp(\alpha d)}{NwI_0} \frac{1}{(t-t_0)} \\ &\quad \times \exp\left[\frac{NwI_0(t-t_0)}{\exp(\alpha d)}\right]. \end{aligned} \quad (4)$$

The variation of  $\alpha_L$  with  $\ln(t-t_0)$  is plotted on Fig. 13. In the intermediate regime, i.e., for  $\tau_{\min} \ll (t-t_0) \ll \tau_{\max}$ , its slope is independent of  $I_0$  and simply equals to  $(\alpha d)^{-1}$ , a parameter which is easy to determine experimentally. The time evolution of the distribution of the magnetization inside the sample as a function of the penetration depth of the light along the  $z$  axis can be estimated (Fig. 14); the pseudolocalized character of the photoinduced magnetic effects produces an

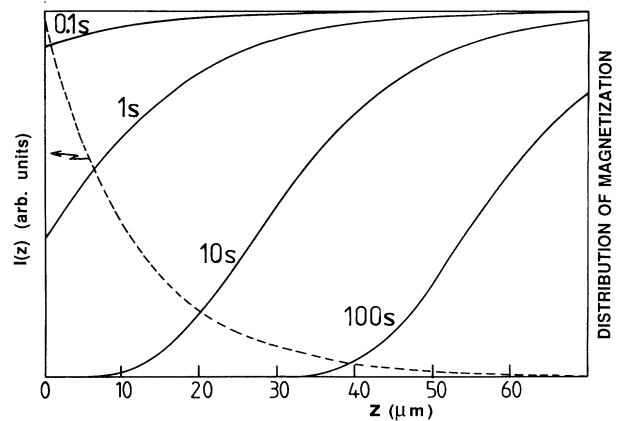


FIG. 14. Distribution of the magnetization as a function of the penetration depth  $z$  (—) in a  $70\text{-}\mu\text{m}$ -thick sample for different characteristic times, using the same values of parameters as that considered in Fig. 13. The exponential decrease of the light intensity inside the sample is also plotted (---).

inhomogeneous distribution of the remanent magnetization in the depth of the sample.

## VI. EXPERIMENTAL JUSTIFICATIONS AND CONSEQUENCES OF THE MODEL

Most of our experiments were performed to check the validity of our theoretical description and to discuss the microscopic origin of the photoinduced effects.

### A. Decoupling between the TRM and the photoinduced magnetic process

The simple expression (3) has to be justified. For this purpose, using an experimental setup arranged in the configuration II (Fig. 9), we have performed the two following experiments (Fig. 15):

- (1) the TRM relaxation is measured under a weak light intensity in the absence of the second light beam;
- (2) the modified relaxation curve is obtained after illumination of the sample by the second source during the time interval  $t_0 < t < t_1$ .

The validation of expression (3) is supported by the following experimental facts:

The additional light-induced relaxation is always fitted by the same  $\alpha_L(t - t_0)$  law whatever the value of  $t_0$  is.

The ratio between magnetization obtained after irradiation of the sample (curve 2) and the TRM in darkness (curve 1) is found to be constant for values of  $t > t_1$ ; it depends only on the relaxation during the time interval  $(t_1 - t_0)$  even if  $t_0 = 0$ . The same result has been obtained for the in-field aftereffect.

The magnetization relaxation law for a sample in darkness for  $t > t_1$  is strongly dependent upon the nature of the inhomogeneous state created after illumination.

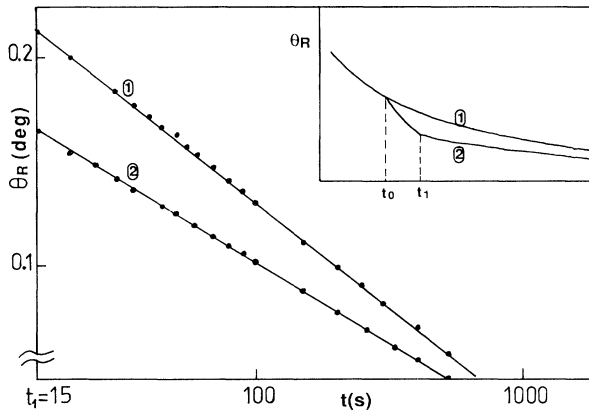


FIG. 15. Time dependence of the thermoremanent Faraday rotation of CoAS 13 ( $T = 1.29$  K,  $H = 3.75$  kOe) in a semilogarithmic plot. It is schematically drawn in the inset as a function of time. Faraday rotation is measured at  $8100 \text{ \AA}$ . The curves (1) and (2) are obtained after relaxation in darkness up to  $t_0 = 10$  s, using a very weak light beam intensity,  $I = 4 \mu\text{W}/\text{mm}^2$ , but (2) alone after illumination of the sample ( $I_0 = 180 \mu\text{W}/\text{mm}^2$ ,  $\lambda = 7500 \text{ \AA}$ ) between  $t_0 = 10$  s and  $t_1 = 15$  s.

The decoupling between the spontaneous and the photoinduced relaxations of the magnetization justifies the above simple analysis of the photomagnetic effect.

### B. Variation with the light intensity

We deduced the  $\alpha_L(t)$  variation (setting  $t_0 = 0$ ) for the CoAS 13 sample (Fig. 16) from the ratio between the photoinduced FR relaxation curves, previously reported in Fig. 2 of Ref. 8, and the TRM Faraday curve measured under low light level, at the same temperature (Fig. 7).

The  $\alpha_L(t)$  curves cannot be fitted by a  $\log t$  law (Fig. 16 and Ref. 9) as for the TRM (Fig. 7). The dependence of  $\alpha_L(t)$  with light intensity is fairly different from that of the TRM( $t$ ) curves with temperature. As expected theoretically,  $\alpha_L$  varies logarithmically with time only in the intermediate time range  $\tau_{\min} \ll t \ll \tau_{\max}$  [expression (4)], the slope being independent of the light intensity  $I_0$ . From Fig. 16 we demonstrate that the  $\alpha_L$  value is only related to the absorbed energy. At short time the set of  $\alpha_L$  curves plotted as a function of  $\log t$  and corresponding to different values of  $I_0$  converges rapidly towards the value  $\alpha_L = 1$ .<sup>9</sup> This strongly supports our model and excludes a rising in temperature of the sample as the origin of such an effect. Moreover, we have verified that the variation of  $\alpha_L(t - t_0, I_0)$  with  $(t - t_0)$  (Fig. 16) or with  $I_0$  gives rise to similar sets of curves, as expected from expressions (4), in which  $(t - t_0)$  and  $I_0$  play the same role.

The value of  $ad$  deduced from the slope of the intermediate regime of the experimental  $\alpha_L$  curves versus  $\log t$  (Fig. 16) is always overestimated. According to the absorption coefficient of our CoAs 13 sample at  $8100 \text{ \AA}$  and to its thickness we deduce  $ad = 4$ , which has to be compared with the experimentally extracted value of 8. This difference can be explained, taking into account of the local character of the photoinduced effect. It is related to

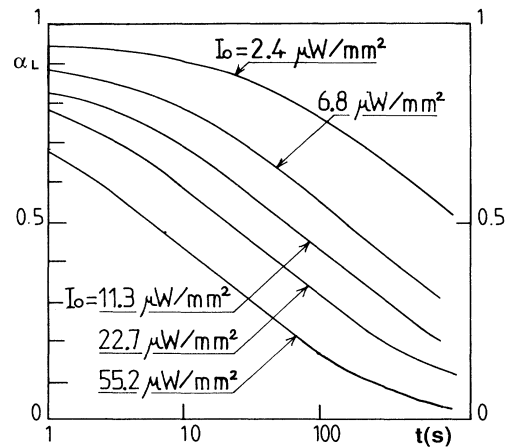


FIG. 16. Time dependence of the photoinduced relaxation coefficient  $\alpha_L$  of CoAS 13 in a semilogarithmic plot, for several values of the light intensity, deduced from experimental curves published in Fig. 2 of Ref. 8 ( $t_0 = 0$ ,  $T = 1.29$  K,  $H = 7.5$  kOe) and from the TRM relaxation curves (Fig. 7).

the fact that we cannot light the sample with an ideal square-shaped spatial distribution of the intensity. Thus, the distribution of light intensity over the beam cross section in the sample generates a distribution of the density

$$\bar{M}(t) = \frac{M_R(t)}{\alpha d} \left\{ \left[ \int_0^{\rho_0} g(\rho) \int_{\tau_{\min}(\rho)}^{\tau_{\max}(\rho)} \left[ \exp - \frac{t}{\tau} \right] \frac{d\tau}{\tau} 2\pi\rho d\rho \right] \right\} / \int_0^{\rho_0} g(\rho) 2\pi\rho d\rho \quad (5)$$

assuming a radial density distribution  $g(\rho)$  up to the radius of the beam cross section  $\rho_0$ .

We experimentally checked the influence of the light beam cross-section profile at constant integrated energy on the photoinduced magnetic relaxation curves (Fig. 17). A sharper distribution of light intensity over the beam section leads to an increase of the apparent slope of the logarithmic regime. This behavior is supported from a simple calculation, assuming a very crude approximation that the light beam cross-section profile can be described by an intensity distribution shown in Fig. 18, i.e., a central part characterized by a power density  $P_1$ , and two limited wings, having the same integrated energy, with power density  $P_2$ . The apparent slope of the logarithmic regime is found to be reduced against the case of a uniform distribution of the intensity over the sample by a factor  $P_2/(P_1 + P_2)$ . These experimental and theoretical arguments well explain the overestimation of  $\alpha d$  from the above-reported data. Such an effect points again the pseudolocalized character of the photoinduced effects, a property directly evidenced in the following section.

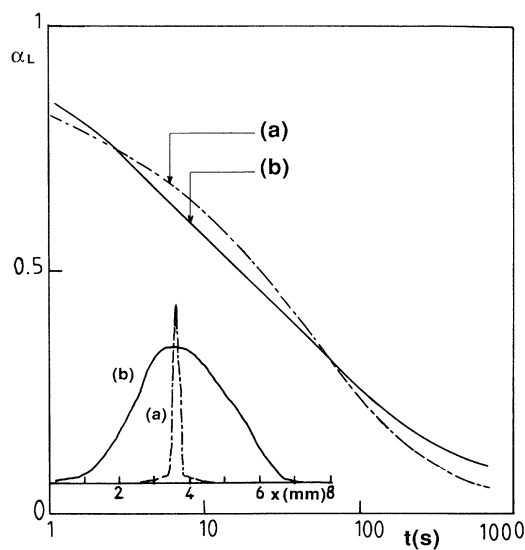


FIG. 17. Variation of the photoinduced magnetic relaxation as a function of the cross-section profile (a) or (b) of the light beam intensity (not normalized) over the sample area ( $I_0 = 90 \mu\text{W}/\text{mm}^2$ ).

of magnetization in wave planes, which is not accounted in Fig. 14. Consequently, assuming  $t_0 = 0$ , the modified averaged magnetization  $\bar{M}(t)$  associated to the Faraday rotation is given by the following expression:

### C. Localization of the photoinduced magnetic effects

For a homogeneous light beam our model predicts a progressive absorption inside the sample which creates a one-dimensional inhomogeneous distribution of the magnetization along the direction of propagation of the light (Fig. 14), conveying the local character of the effect.

To check the localization of the photoinduced magnetic effects more directly than in Sec. III we followed the time dependence of the spatial distribution of the remanent magnetization of the CoAS 13 sample, created by an inhomogeneous light beam profile having a nearly Lorentzian shape (Fig. 19).<sup>10</sup> A part of the area of a thin sample plate ( $e = 70 \mu\text{m}$ ) was first illuminated ( $I_0 = 180 \mu\text{W}/\text{mm}^2$ ) during 1 min after switching off the magnetic field. For several values of the waiting time  $t$ , we measured the distribution of the magnetization by Faraday rotation, scanning the attenuated light beam ( $I_0 = 2 \mu\text{W}/\text{mm}^2$ ) over the sample (Fig. 19). The inhomogeneous distribution of the Faraday rotation has the same shape as the light beam intensity profile, estimated in a logarithmic scale. No change of the shape of the distribution of the magnetization has been evidenced, even after waiting a long time; the localization of the photoinduced effect is consequently estimated to be better than  $50 \mu\text{m}$ . These facts confirm the absence of connection between the spontaneous and of the optically induced relaxation processes.

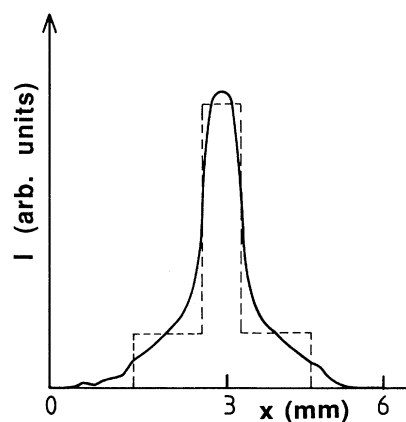


FIG. 18. Real shape of the light beam cross-section intensity (—) and its crude approximations (---) used in the discussion.

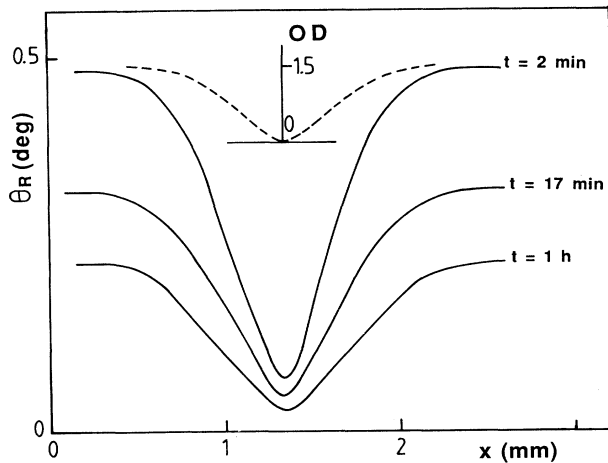


FIG. 19. Inhomogeneous distribution of the remanent Faraday rotation of CoAS 13 (—) along the  $x$  axis located in the plane of the sample, created by a previous 1 min light illumination at  $\lambda = 8100 \text{ \AA}$ , plotted for different waiting times  $t$  in darkness. Measurements were performed at 1.29 K, after cooling the sample in  $H = 7.5 \text{ kOe}$ . The intensity profile of the light spot in a logarithmic scale is also presented (---).

#### D. Variation of the photoinduced "dynamic magnetic correlation length" with the applied magnetic field

The model we proposed, based on a finite mean value of the photoinduced "dynamic magnetic correlation length," explains our data well. Nevertheless, to get a better description of the mechanism responsible for this effect, we need more information on this typical length and in particular on its temperature and field dependence.

Starting from the same value of the applied magnetic

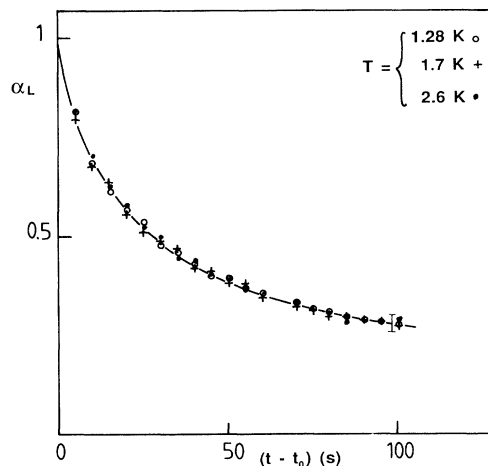


FIG. 20. Photoinduced relaxation of the magnetization of CoAS 13 at different temperatures (the initially applied field value was 3.75 kOe).

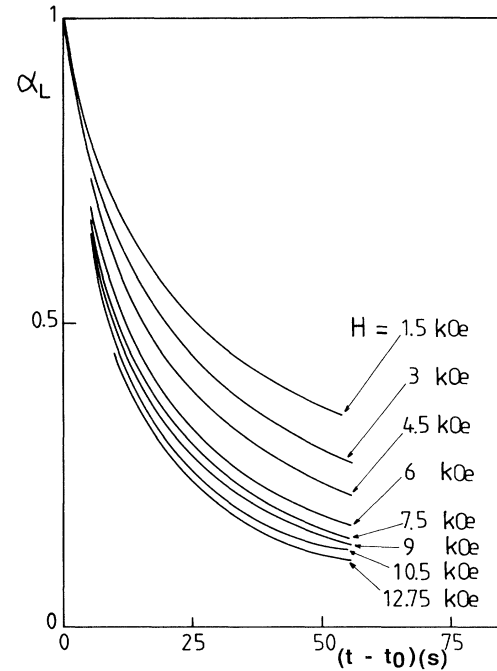


FIG. 21. In-field photoinduced magnetic aftereffect of CoAS 13 obtained for different applied field values at 1.45 K.

field, we demonstrated that the photoinduced relaxation  $\alpha_L(t - t_0)$  of the TRM does not depend on the temperature between 1.28 and 2.6 K (Fig. 20), and of the value of the initially applied field, which means no variation of the correlation length with temperature and magnetic preparation of the sample before switching off the field. On the contrary, the magnetic correlation length is slightly increased under magnetic field as demonstrated by the in-field aftereffect (Fig. 21).

As demonstrated before, the amorphous structure is needed to generate photoinduced magnetic effects in spin glasses. However, frustration is certainly an important parameter which limits the photoinduced "dynamic magnetic correlation length." The acceleration of the photoinduced relaxation can be correlated with a reduction of the frustration under field, as often admitted in spin glasses.

#### E. Dependence of the photoinduced magnetic effect on the wavelength of the radiation

We have shown that the photomagnetism in CoAS 13 appears at all light wavelengths in the optical range 0.4–2.5  $\mu\text{m}$  and that it is not related to one particular optical transition (Fig. 2). The dependence of the photoinduced relaxation of the magnetization with the irradiation wavelength for the same light energy is shown in Fig. 22, using an experimental setup in configuration II (Fig. 9). As predicted theoretically by expressions (4), the light efficiency becomes stronger when the absorption coefficient  $\alpha$  decreases and is maximum in the transparency window ( $\sim 0.8 \mu\text{m}$ ) between the two main absorption

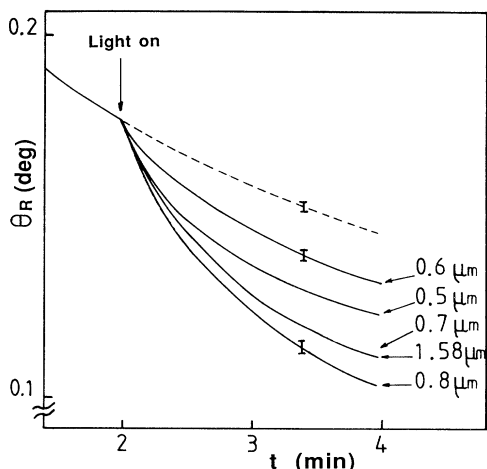


FIG. 22. Variation of the photoinduced relaxation of the magnetization of CoAS 13 with the radiation wavelength at constant light energy ( $I_0 = 100 \mu\text{W}/\text{mm}^2$ ).

bands. From these data we do not expect a large variation of the number of magnetic ions  $N$  (or of the correlation length) and of the atomic cross section  $w$  with light wavelength. All these results are also found valid for the manganese compound MnAS 18. We conclude that the photoinduced magnetic phenomenon is mainly related to the absorption coefficient value and does not depend upon the origin of the involved electronic states in the optical transition process.

## VII. DISCUSSION ON THE MICROSCOPIC ORIGIN AND CONCLUSIONS

Only spin glasses with amorphous structure exhibit photomagnetism<sup>8,11</sup>; the microscopic origin of this effect has to take into account the glass structure and the particular magnetic lattice topology. Moreover, our spectroscopic analysis excludes the usually invoked origin for photoinduced magnetic phenomena, i.e., the presence of magnetic ions in two different valence states<sup>1-7</sup>; a new mechanism has to be put forward. Since the metal ions are orbitally quenched (see Sec. II A 2), the local magnetic anisotropy is very weak in these glasses and it cannot be at the origin of the photomagnetism as in some doped garnets.<sup>7</sup>

As demonstrated experimentally above, sample heating by light absorption cannot explain the observed phenomenon. A simple calculation based on the thermal conductivity equation

$$\frac{\delta Q}{\delta t} = \frac{K \Delta T}{e} \quad (6)$$

allows a crude estimation of the rise in temperature  $\Delta T$ . In this equation  $Q$  is the thermal energy per unit deposited by the light beam,  $K$  is the thermal conductivity, and  $e$  the sample thickness. For the cobalt glass CoAS 13 at 1.29 K the thermal conductivity is of the order of  $10^{-3} \text{ W cm}^{-1} \text{ K}^{-1}$ . Taking a typical laser power of  $100 \mu\text{W}$

and a beam cross section on the sample of  $2.7 \text{ mm}^2$ , the rise in temperature is calculated to be less than  $10^{-2} \text{ K}$ . It is not large enough to produce any observable effects on the magnetic properties of this material (see Fig. 7). This last treatment neglects the transient processes, which leads to thermal equilibrium and assumes a thermalized phonon bath. If this hypothesis can be valid in crystals, it falls down in glasses, where localization of elementary excitations becomes possible as a consequence of the loss of translation symmetry. Numerous experimental methods like small-angle x-ray scattering,<sup>31</sup> dark field microscopy,<sup>32</sup> or Raman scattering<sup>33</sup> evidence the presence of microregions with structural correlations of typical size  $L_{\text{SC}} = 10-20 \text{ \AA}$  (Ref. 34) in amorphous solids and glasses, which provides the localization of elementary excitations.

In glasses, the dynamical properties are drastically different from that expected for pure crystals. The excitation energy transfer from the electron subsystem to the lattice takes place in two steps: first, high-energy phonons are locally emitted and afterwards they diffuse in the host material by phonon-phonon interaction. This last thermalization process of the phonon bath needs a fraction of a second. Note again that the corresponding rise in temperature due to light irradiation is weak in our case. The radiationless transitions of manganese or cobalt in our glasses are related to multiphonon emission processes. Since the thermal diffusion in the glass is slow and the light emission lifetime long enough (few milliseconds, as mentioned in Sec. II B 3), the nonthermalized high-energy phonons remain localized around metallic ions which increase considerably the local "effective temperature"  $T_{\text{eff}}$  of the spin system. Such a mechanism has been already proposed to explain the formation of laser-induced permanent gratings in Eu-doped glasses.<sup>35</sup> For an estimation of  $T_{\text{eff}}$  we can assume, in a first approximation, that phonons localized in microregions surrounding the photoexcited ions are characterized by a mean characteristic frequency  $\omega = 2\pi v / L_{\text{SC}}$ , if  $v$  stands for the sound velocity in the medium. For oxide glasses  $\omega$  corresponds to energies between  $700$  and  $1400 \text{ cm}^{-1}$ .<sup>34</sup> The number of localized phonons created in this microregion during a time  $\tau_L$  is given by

$$\Delta n(\omega) = \frac{P V_{\text{SC}} W_{\text{nr}} \tau_L}{V_c h \nu}, \quad (7)$$

where  $P$  represents the absorbed light power at frequency  $\nu$ ,  $W_{\text{nr}}$  is the probability for nonradiative processes,  $V_c$  stands for the irradiated sample volume, and  $V_{\text{SC}}$  is the volume of a crystalline microregion. Since the quantum yield of fluorescence is very weak in our samples, we expect a large value for  $W_{\text{nr}}$ , which can be taken as 1.

Assuming a Bose-Einstein distribution for phonons,  $T_{\text{eff}}$  can be expressed by

$$T_{\text{eff}} = \hbar \omega / \left\{ k \ln \left[ \left[ \Delta n(\omega) + \frac{1}{\exp(\hbar \omega / kT - 1)} \right]^{-1} + 1 \right] \right\} \quad (8)$$

if  $k$  stands for the Boltzmann constant and  $T$  is the equilibrium temperature of the host material. Taking  $\omega = 1000 \text{ cm}^{-1}$ ,  $P = 100 \text{ } \mu\text{W}$ , the calculated value of the "effective temperature,"  $T_{\text{eff}} = 15 \text{ K}$ , is far greater than the freezing temperature of the CoAS 13 sample. Thus the effect of localization of high-frequency vibrations around the optically excited metal ion is to rise the "effective temperature" in microregions of typical size  $10\text{--}20 \text{ \AA}$  in which the remanent magnetization is rapidly annealed.

However, in contrast with high-frequency phonons, this local magnetic perturbation can diffuse away from these microregions via the large Co-Co exchange interaction which involves a characteristic time  $\tau_{\text{ex}} \approx \hbar / J \approx 10^{-13} \text{ s}$  shorter than typical periods of local vibrations ( $10^{-11} \text{ s}$ ). This supports the concept of a "dynamical magnetic correlation length" and the localization of the magnetic excitation. However, the ramified character of the magnetic lattice, which is topologically related to the glass network (see Sec. III), leads to a correlation length larger than  $L_{\text{SC}}$ .

In conclusion, to interpret the photoinduced magnetic effect in amorphous spin glasses we developed a semi-phenomenological model whose hypotheses have been experimentally verified. As pointed out previously,<sup>8</sup> this photoinduced effect may be very useful to reach the equilibrium state of the system rapidly without heating the whole sample above  $T_f$ . As discussed above, the most probable origin of this phenomenon, which takes into account of the particular lattice structure of amorphous material, is an increase of the local effective temperature in the surrounding of an optically excited magnetic ion. The "dynamic magnetic correlation length" is then related to the degree of frustration of the magnetic interactions and consequently depends upon the value of the ap-

plied field. Other mechanisms cannot be definitively ruled out, such as a direct strong modification of the local exchange interaction between excited magnetic ions or its indirect change from local distortions induced by magnetoelastic coupling. If in these processes one spin is reversed, the metastability of the TRM can be easily affected to get a complete demagnetization in a localized microregion. However, this last mechanism can occur also in crystalline materials.

Complementary experiments on amorphous metallic alloy spin glasses<sup>11</sup> are highly desirable to confirm our model. Magneto-optical experiments at very short times might be useful to investigate the microscopic mechanism in more details and in particular to probe the role of radiationless processes in the excited state.

#### ACKNOWLEDGMENTS

We are grateful to Professor A. M. de Graaf, L. W. Wenger (Wayne State University, Chicago), and K. Knorr (Univ. Tübingen) for lending us the cobalt and manganese samples, respectively. X-ray absorption experiments were performed at LURE (Orsay). We wish to thank G. Calas, J. Petiau (Univ. Paris VI), and A. Le Bail (Univ. Le Mans) for their advice and fruitful discussions on EXAFS results. We also acknowledge G. Colliex, M. Tancé, and P. Ballongue (Univ. Orsay) for their invaluable advice in electron microscopy measurements. We are grateful to the researchers of the J. P. Renard group at the IEF Laboratory (Orsay) for their help in performing extraction magnetization measurements. This work could not have been realized without the assistance of A. Boix. The Laboratoire de Physique des Solides is associated with the CNRS.

\* Author to whom correspondence should be addressed.

- <sup>1</sup>R. W. Teale and D. W. Temple, *Phys. Rev. Lett.* **19**, 904 (1967).
- <sup>2</sup>U. Enz, R. Metselaar, and P. J. Rijnierse, *J. Phys. (Paris) C* **1**, 703 (1970); V. F. Kovalenko and E. L. Nagaev, *Usp. Fiz. Nauk* **148**, 561 (1986) [*Sov. Phys. Usp.* **29**, 297 (1986)].
- <sup>3</sup>W. Lems, P. J. Rijnierse, P. F. Bongers, and U. Enz, *Phys. Rev. Lett.* **21**, 1643 (1968).
- <sup>4</sup>H. D. Jonker, *J. Solid State Chem.* **10**, 116 (1974).
- <sup>5</sup>D. E. Lacklison, J. Chadwick, and J. L. Page, *J. Phys. D* **5**, 810 (1972).
- <sup>6</sup>J. F. Dillon, E. M. Gyorgy, and J. P. Remeika, *Phys. Rev. Lett.* **23**, 643 (1969).
- <sup>7</sup>E. M. Gyorgy, J. F. Dillon, and J. P. Remeika, *J. Appl. Phys.* **42**, 1454 (1971).
- <sup>8</sup>M. Ayadi and J. Ferré, *Phys. Rev. Lett.* **50**, 274 (1983).
- <sup>9</sup>J. Ferré and M. Ayadi, *J. Appl. Phys.* **55**, 1720 (1984).
- <sup>10</sup>M. Ayadi and J. Ferré, *J. Magn. Magn. Mater.* **54-57**, 91 (1986).
- <sup>11</sup>C. J. O'Connor and J. F. Noonan, *J. Phys. Chem. Solids* **48**, 303 (1987).
- <sup>12</sup>R. A. Verhelst, R. W. Kline, and A. M. de Graaf, *Phys. Rev. B* **11**, 4427 (1975).
- <sup>13</sup>K. Knorr, R. Geller, and W. Prandl, *J. Magn. Magn. Mater.* **4**, 258 (1977).

- <sup>14</sup>Y. H. Wong, D. Thomas, R. Thomas, and P. S. Danielson, *J. Appl. Phys.* **49**, 1640 (1978).
- <sup>15</sup>J. Ferré, J. Pommier, I. R. Jahn, and Y. Tanabe, *Solid State Commun.* **33**, 27 (1980).
- <sup>16</sup>G. Calas and J. Petiau, *J. Phys. (Paris) Suppl. No.* **12**, 47 (1982).
- <sup>17</sup>W. Nagele, K. Knorr, W. Prandl, P. Convert, and J. L. Buevos, *J. Phys. C* **11**, 3295 (1978).
- <sup>18</sup>J. P. Jamet, J. C. Dumais, J. Seiden, and K. Knorr, *J. Magn. Magn. Mater.* **15-18**, 197 (1980).
- <sup>19</sup>R. Pappalardo, D. L. Wood, and R. C. Linares, *J. Chem. Phys.* **35**, 2041 (1961).
- <sup>20</sup>J. Ferré, M. Ayadi, and J. Pommier (unpublished results).
- <sup>21</sup>J. Ferré, J. Pommier, J. P. Renard, and K. Knorr, *J. Phys. C* **13**, 3697 (1980).
- <sup>22</sup>P. Beauvillain, C. Dupas, J. P. Renard, and P. Veillet, *Phys. Rev. B* **29**, 4086 (1984).
- <sup>23</sup>L. E. Wenger, in *Proceedings Heidelberg Colloquium on Spin Glasses*, edited by J. L. Van Hemmen and I. Morgenstern (Springer, Heidelberg, 1983), p. 60.
- <sup>24</sup>L. E. Wenger and J. A. Mydosh, *J. Appl. Phys.* **55**, 1717 (1984).
- <sup>25</sup>T. Wang, H. V. Bohm, and L. E. Wenger, *J. Magn. Magn. Mater.* **54-57**, 89 (1986).

- <sup>26</sup>W. Kleemann, F. J. Schafer, and J. Ferré, *J. Magn. Magn. Mater.* **54-57**, 1289 (1986).
- <sup>27</sup>J. Ferré, R. Rajchenbach, and H. Maletta, *J. Appl. Phys.* **52**, 1697 (1981).
- <sup>28</sup>J. Pommier, J. Ferré, and S. Senoussi, *J. Phys. C* **17**, 5621 (1984).
- <sup>29</sup>J. Ferré and N. Bontemps, in *Materials Science Forum* (Trans. Tech. Publications, Switzerland, 1990), No. 50, p. 21.
- <sup>30</sup>J. Souletie, *J. Phys. (Paris) Colloq.* **39**, C2-3 (1978); M. Cyrot, *Phys. Rev. Lett.* **43**, 173 (1979).
- <sup>31</sup>P. Antonio and I. H. Konnert, *Phys. Rev. Lett.* **43**, 1161 (1979).
- <sup>32</sup>P. Chandari, I. F. Graczyck, and H. P. Charban, *Phys. Rev. Lett.* **29**, 425 (1972).
- <sup>33</sup>A. J. Martin and W. Bring, *Phys. Status Solidi* **6**, 163 (1974).
- <sup>34</sup>J. C. Phillips, *J. Non-Cryst. Solids* **43**, 37 (1981).
- <sup>35</sup>F. M. Durville, E. G. Behrens, and R. C. Powell, *Phys. Rev. B* **34**, 4213 (1986).

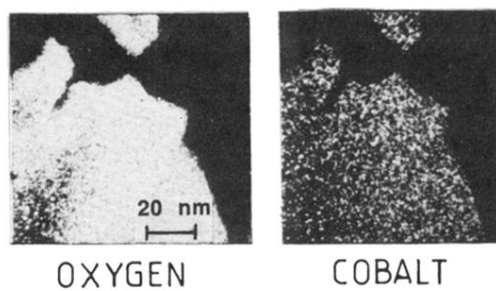


FIG. 1. Distribution of oxygen and cobalt (13 at. %) atoms in CoAS 13 (STEM measurements). The short-range contrast is mainly due to the noise.